| | |
|---|---|
| **Titre:** Title: | Enhancing seafood freshness monitoring : integrating color change of a food-safe on-package colorimetric sensor with mathematical models, microbiological and chemical analyses. Supplément |
| **Auteurs:** Authors: | Maryam Ameri, Abdellah Ajji, & Samuel Kessler |
| **Date:** | 2024 |
| **Type:** | Article de revue / Article |
| **Référence:** Citation: | Ameri, M., Ajji, A., & Kessler, S. (2024). Enhancing seafood freshness monitoring : integrating color change of a food-safe on-package colorimetric sensor with mathematical models, microbiological and chemical analyses. Current Research in Food Science, 9, 100934 (15 pages). https://doi.org/10.1016/j.crfs.2024.100934 |



| | |
|---|---|
| **Titre de la revue:** Journal Title: | Current Research in Food Science (vol. 9) |
| **Maison d'édition:** Publisher: | Elsevier |
| **URL officiel:** Official URL: | https://doi.org/10.1016/j.crfs.2024.100934 |
| **Mention légale:** Legal notice: | |

## Supplementary materials

FTIR measurements confirmed hydroxyl, carboxylic, and ester groups. **Figure 1 (a)** shows the Ink ingredients and prepared INK I. **Figure 1 (b)** shows the developed pH indicators (Ink I-NTT and Ink I-165-5). All samples showed similar behavior, with bands in the 3400–3200 $cm^{-1}$ range due to the O-H group's stretching vibration[1,2]. In PVOH, the absorption band around 1638 $cm^{-1}$ is due to C=O stretching vibrations, indicative of the presence of residual carbonyl groups in the polymer backbone[3]. The 1638 (C-O stretching) and 1572/1517 bands indicate roasted black rice protein. The C-H bending vibration bands were 1441–1323 $cm^{-1}$, while the O-H band was 1242 $cm^{-1}$ [4]. The bands at 1157 and 1008 $cm^{-1}$ were ring vibrations displayed with lateral group stretching vibrations (C-OH) and C-O-C glycoside vibrations[5]. In CA, two peaks at approximately 1745 and 1700 $cm^{-1}$ could be attributed to the C=O stretching[1]. In PEG, the band observed at approximately 2875 $cm^{-1}$ and peak 1466 $cm^{-1}$ were attributed to the C-H stretching and C-H bending vibrations of the -$CH_2$ group of ethylene glycol, respectively[2]. Other peaks also observed at 1245, 1051, 944 and 874 $cm^{-1}$ [2] . In prepared INK 1, there is a new peak (approximately at 1600 $cm^{-1}$) that can be attributed to the interaction between black rice, PEG, and CA.

In coated PET films with INK I formulation, a new peak at 2919 $cm^{-1}$ may be owing to PEG bridging PVOH groups. Temperature treatment reduces hydroxyl band intensity, indicating water loss and fewer water molecules available for hydrogen bonding due to dehydration. Absorption of 1713 $cm^{-1}$ is attributed to C=O stretching vibrations from coated film carbonyl groups. The esterification is supported by Fisher's esterification's 1230 $cm^{-1}$ band[6]. This peak shows CA-PVOH crosslinking**.**

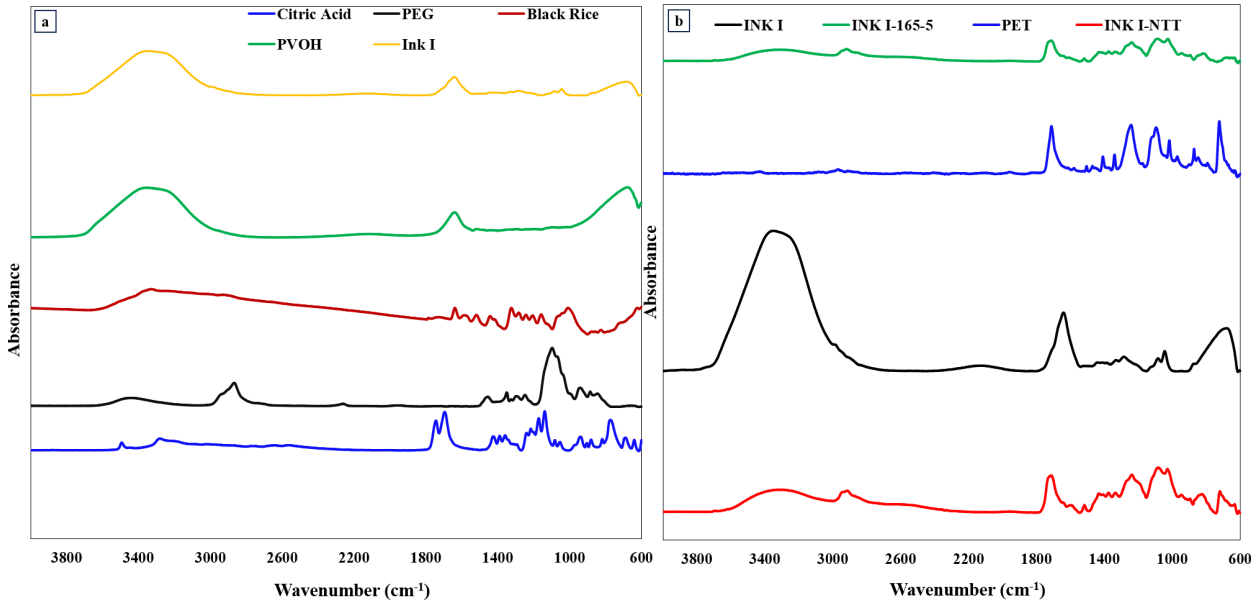


**Figure 1** FTIR-spectra of each component of formulated ink solution (Ink I) (a) and produced colorimetric films with and without thermal treatment (INK I-165-60, INK-I-NTT), and PET film (b).

**Signal response against Ammonia gas**

A scanner recorded the color change of the colorimetric films before and after a 24-hour exposure to ammonia gas in combination with water vapor, which forms ammonium hydroxide. The colorimetric films were placed inside the containers with an inlet to pour Ammonium hydroxide solution. After introducing the ammonium hydroxide, we quickly capped the inlet and sealed the container to avoid any leakage. Then the ammonium solution under a reversible equilibrium equation can change its form to ammonia gas and water. **Figure 2** demonstrates that the developed sensors effectively change color due to the exposure of nitrogen-based components (such as $NH_3$) during fish spoilage. Other TVB-N gases sensing capability also checked with exact description in our pervious study[7].

The storage stability of pH indicators that have undergone thermal treatment is superior to that of untreated indicators when exposed to humid environments. However, their detection capacity is limited to 5 µL of the solution stock. In addition, the pH indicators exhibited a rapid color shift upon the introduction of 25 µL of the base solution to their headspace. The response time of pH indicator (165–5) was around one minute after the addition of 5 µL of the base solution. The lag time in color change for thermally treated pH indicators can indeed be attributed to a slight degradation that affects the active sites (specific chemical groups that can interact with hydrogen ions or hydroxide ions) responsible for the acid-base reactions. Thus, with fewer active sites available, the pH indicator may not respond immediately to changes in pH. This results in a lag time, as it takes longer for the available active sites to interact sufficiently with the ions in the solution to cause a noticeable color change. Also, there is a correlation between surface polarity and the pH sensing response; as the hydrophilicity of the pH indicator surface increases, the response time will increase[8]. As in our previous study, we documented that, through thermal treatment procedure, the surface of pH indicators becomes more hydrophilic[7].

Crosslinking networks could also explain this observation. These networks made it harder for the analyte (in this case, ammonia gas) to diffuse, which made the dye less effective at binding to the analyte[8].

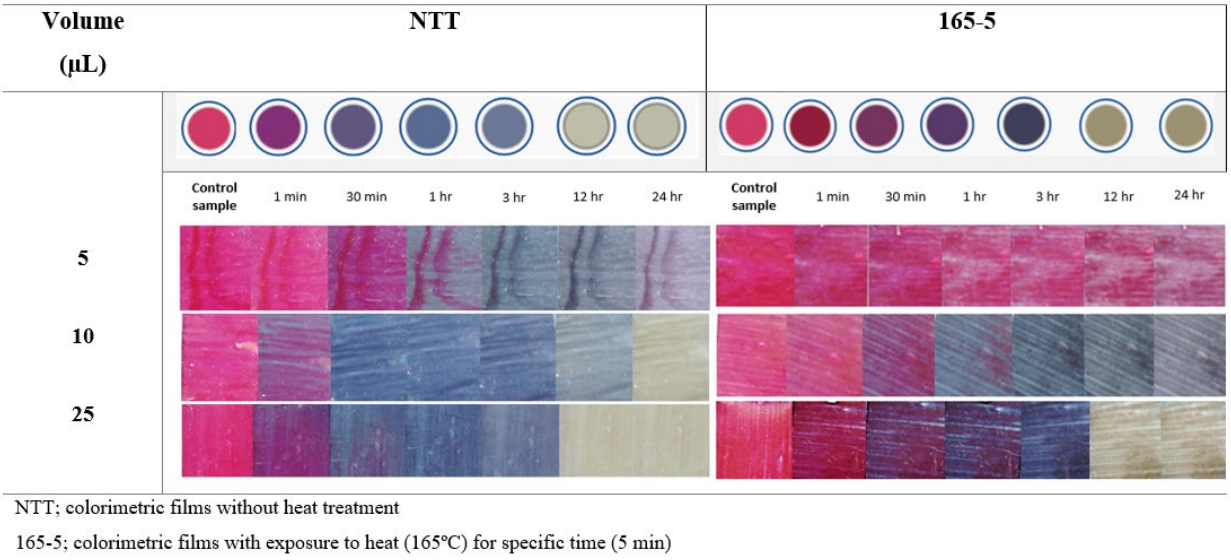


**Figure 2** Color change of the colorimetric films with and without thermal treatment (INK I-165-60, INK-I-NTT) when exposed to different volumes of the same ammonia concentration.

**Figure 3** illustrated the ΔRGB (color change) response of the pH sensor to various weights of fish samples (30, 50 and 100 gr) stored over nine days in packages with different pH indicators (NTT and 165-5). According to the observations, the different weights and conditions of the fish samples impacting sensor response exhibit varying levels of sensitivity, as indicated by the range of ΔRGB values.

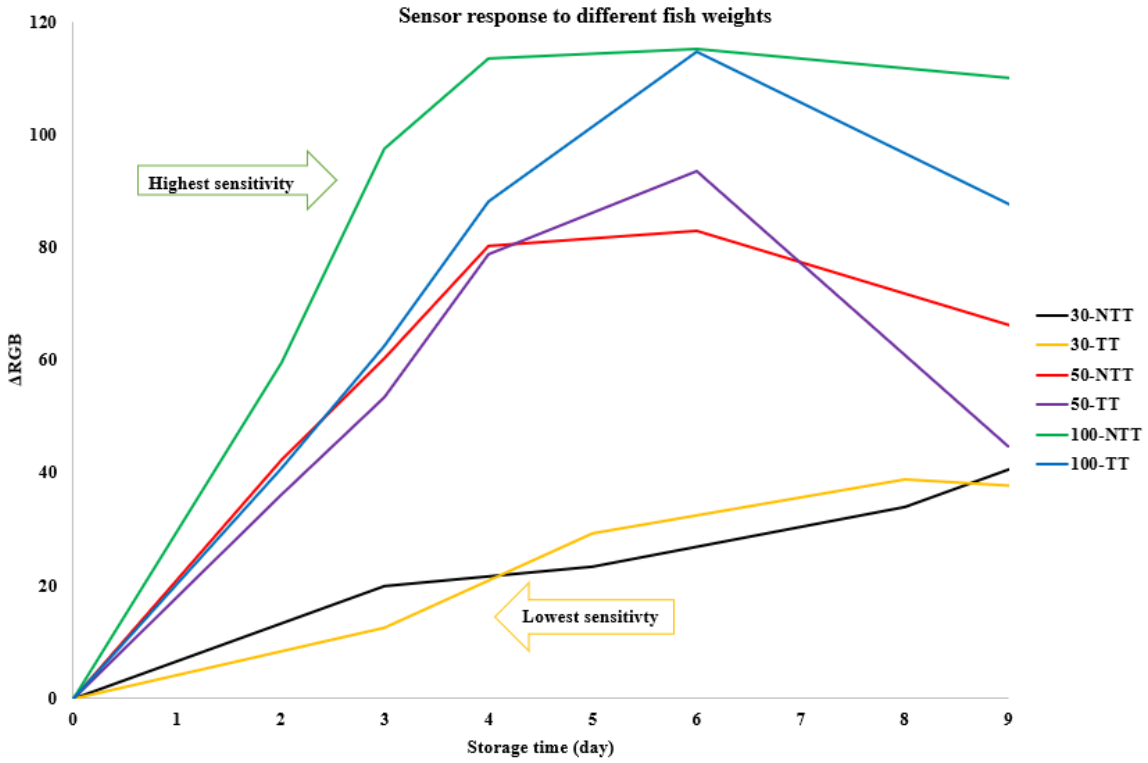


**Figure 3** Sensor Response to Different Fish Weights Over Storage Time.

## Chemical stability and Recovery tests

Important attributes of intelligent gas sensors include high sensitivity and immediate reaction to gas vapors, exhibit a distinct color change, as well as the ability of indicator films to be reversed[9,10]. The reversibility of the indicator films was tested by exposing the films repeatedly to a defined volume of ammonia and Hydrochloric acid vapors for 3 min each as described [9].

**Table 1** standard dilutions for TMA: 0, 0.025, 0.125, 0.25, 0.5, 0.75, 1, 1.25, 1.5 (wt/wt) for storage condition (T= 60 ºc for 30 minutes).

| | Concentration | Mean R | Mean G | Mean B | Std R | Std G | Std B | Hue (degrees) |
|---|---|---|---|---|---|---|---|---|
| | 0 | 157.24 | 88.23 | 114.67 | 79.47 | 58.49 | 76.44 | 342.02 |
| | 1 | 170.39 | 64.07 | 104.89 | 87.83 | 39.17 | 53.94 | 344.24 |

| | | | | | | | | |
|---|---|---|---|---|---|---|---|---|
| TMA | 2 | 160.19 | 86.08 | 113.38 | 82.88 | 46.57 | 59.29 | 340.88 |
| | 3 | 160.75 | 103.58 | 126.02 | 83 | 53.97 | 65.64 | 341.37 |
| | 4 | 162.59 | 103.17 | 132.33 | 83.7 | 53.14 | 68.34 | 335.95 |
| | 5 | 187 | 115 | 149 | 18.01 | 40.61 | 35.6 | 328.41 |
| | 6 | 186.98 | 139.31 | 158.37 | 51.23 | 39.42 | 43.59 | 322.65 |
| | 7 | 187.56 | 140.06 | 159.09 | 51.77 | 39.94 | 44.02 | 322.8 |
| | 8 | 189.89 | 143.87 | 163.67 | 53.62 | 41.67 | 46.27 | 319.4 |

**Table 2** standard dilutions for DMA: 0, 0.025, 0.125, 0.25, 0.5, 0.75, 1, 1.25, 1.5 (wt/wt) for storage condition (T= 60 ºc for 30 minutes).

| | Concentration | Mean R | Mean G | Mean B | Std R | Std G | Std B | Hue |
|---|---|---|---|---|---|---|---|---|
| DMA | 0 | 157.24 | 88.23 | 114.67 | 79.47 | 58.49 | 76.44 | 337.01 |
| | 1 | 167 | 147 | 169 | 61.14 | 55.31 | 56.31 | 294.55 |
| | 2 | 167 | 146 | 167 | 15.79 | 19.16 | 18.64 | 300 |
| | 3 | 158.45 | 139.78 | 159.75 | 15.83 | 19.72 | 18.87 | 296.09 |
| | 4 | 104.3 | 98.22 | 111.98 | 53.87 | 51.19 | 57.75 | 266.51 |
| | 5 | 137.57 | 137.46 | 142.27 | 17.95 | 19.5 | 21.39 | 241.37 |
| | 6 | 136.1 | 119.81 | 137.74 | 68.65 | 61.05 | 69.62 | 294.51 |
| | 7 | 141.97 | 138.74 | 143.54 | 22.58 | 23.12 | 23.81 | 280.38 |
| | 8 | 137.78 | 135.23 | 139.54 | 21.53 | 21.81 | 22.55 | 275.5 |

**Table 3** standard dilutions for $NH_3$: 0, 0.025, 0.125, 0.25, 0.5, 0.75, 1, 1.25, 1.5 (wt/wt) for storage condition (T= 60 ºc for 30 minutes).

| | Concentration | Mean R | Mean G | Mean B | Std R | Std G | Std B | Hue (degrees) |
|---|---|---|---|---|---|---|---|---|
| $NH_3$ | 0 | 157.24 | 0 | 60 | 79.47 | 58.49 | 76.44 | 337.11 |
| | 1 | 149 | 49 | 99 | 18.6 | 18.68 | 18.33 | 330 |
| | 2 | 149 | 81 | 29 | 15.4 | 15.98 | 16.67 | 26 |
| | 3 | 115 | 76 | 112 | 12.48 | 19.29 | 19.49 | 304.62 |
| | 4 | 131.29 | 93.92 | 132.71 | 12.64 | 14.23 | 13.36 | 297.8 |
| | 5 | 129 | 120 | 151 | 10.71 | 23.6 | 17.77 | 257.42 |
| | 6 | 95 | 91 | 122 | 15.31 | 25.24 | 20.2 | 247.74 |
| | 7 | 98.17 | 96.33 | 130.3 | 15.29 | 14.81 | 16.11 | 243.25 |
| | 8 | 107.38 | 108.14 | 143.96 | 17.23 | 16.66 | 15.58 | 238.75 |

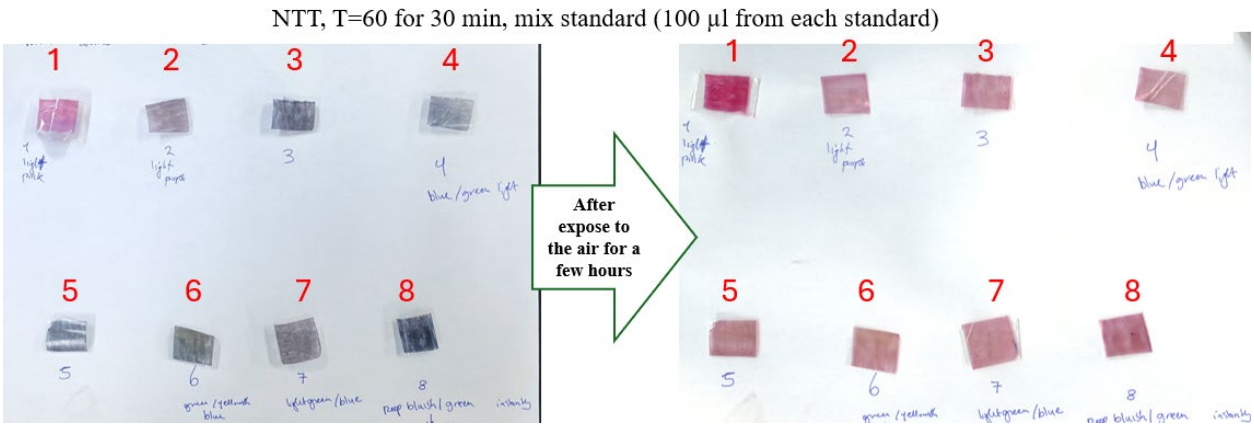


**Figure 4** Sensitivity trials for NTT pH indicators at T=60º C for 30 minutes.

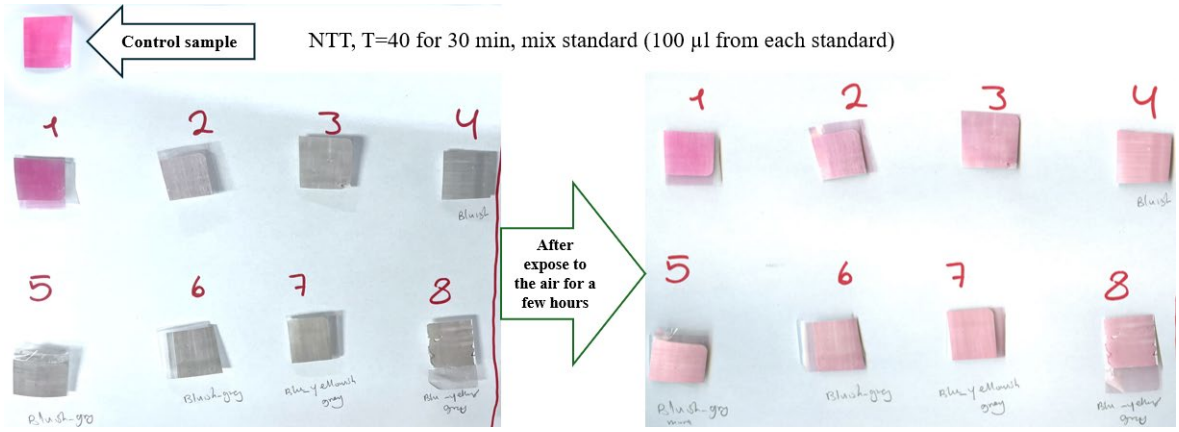


**Figure 5** Sensitivity trials for NTT pH indicators at T=40º C for 30 minutes

## Mathematical model for shelf-life predication based on the experimental data

At the last step, the mathematical models were employed to experimental data to predicate the fish spoilage. The modified logistic and Howgate models provide superior performance in predicting TVB-N gas, while the modified Arrhenius models demonstrate greater performance in predicting bacterial population. The mean value of six experimental data points for TVB-N levels provides some insights but does not capture the system's full variability and complexity. With an inadequate number of samples, error estimation (RMSE and AIC) may be unreliable, and the model may overfit or underfit. Model validation requires enough data points, but splitting a limited dataset for validation is a challenge.

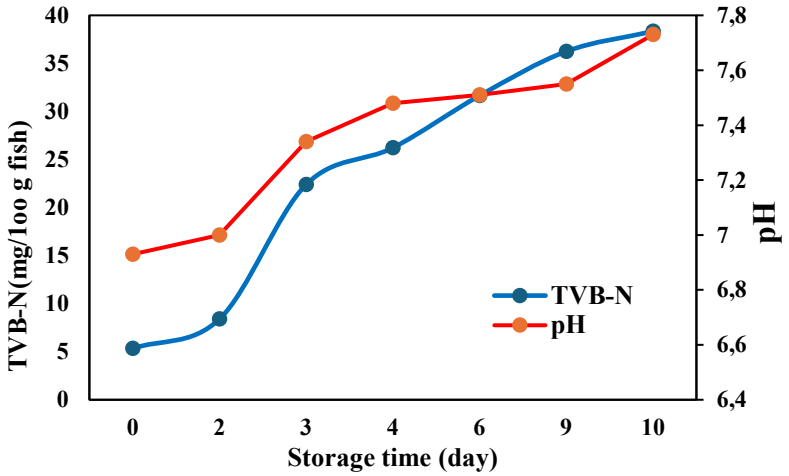


**Figure 6** TVB-N content and pH level of fish fillet during the storage time at 4 ºC.

## Mathematical model for TVB-N and Interpretation of Metrics

The simulation models were fitted using the experimental TVB-N values (mean) of Pangasius fish during storage to predict their release. According to the literature, an experimental model is suggested for storage temperatures ranging from 5 to 4 ºC[11]. However, the exponential model showed the least satisfactory results, due to high RMSE and AIC compared to other models (Modified logistic and Exponential polynomial). The observed low fitting exponential model in the stored samples may be attributed to several factors, including changes in the composition of microbial activity over time, chemical interactions between TVB-N gases and other compounds in the headspace of fish samples, and the volatilization and adsorption of TVB-N gases on the surface of the fish containers during storage. The exponential model has less explanatory power. Improved the model performance were performed by Introducing a quadratic term ($Bt^2$) in the exponential model, significantly improved its performance by lowering the RMSE and AIC metrics, highlighting the need for incorporating additional terms to better capture the underlying processes[12]. Since, the observed data points had an S shape curve similar to the exponential growth function, the modified logistic function is also explored as a potential model for formation of TVB-N gases during fish spoilage at 4 ºC. To employ the Howgate model, we needed to parametrize $Y_{max}$, $Y_{min}$, K, and td. However, the fitting algorithm did not converge due to the limited number of observational and experimental data points. Therefore, we assumed, entered $Y_{min}$ as the initial value, and then proceeded to parametrize the remaining parameters. The study found that the Howgate, modified logistic, and exponential polynomials had lower RMSEs of 2.28, 2.29, and 2.88 than all the other models that were fitted to the experimental data. A lower RMSE indicates better predictive accuracy. We also obtained lower AIC values, which can suggest better model parsimony: 34.95 for both the Howgate and modified logistic models, and 37.74 for the exponential polynomial model. **Table 4** summarizes the model parameters along with goodness of fit metrics. Therefore, the Modified logistic model and Howgate showed the best fitting performance with lowest AIC and RMSE among the models. In comparison, the modified logistic model has a reduced number of parameters and requires fewer assumptions to develop predictions. Noticeably, the A, K parameters of the Modified logistic model and $Y_{max}$ ,$t_d$ and K are statistically significant with p-values below 0.01 and 0.05 respectively.

## Mathematical model for TVC, pseudomonas spp and Interpretation of Metrics

Food safety and quality can also be assessed using predictive microbiology instead of traditional methods. As storage conditions can alter spoiling microorganisms, we used TVC data points for fitting with available kinetic models. Initially, the logistic and modified logistic as three-parameter models were applied to the microbiological experimental data of the present study. Subsequently, the modified Gompertz model (four-parameter) were fitted[11]. In modified Gompertz model, $\mu_{Max}$ has estimated ($0.6649 \pm 0.14$ $day^{-1}$) and statistically significant at p-value < 0.01[13-15]. A "lag time" is the amount of time it takes to achieve a 50% or 100% increase. We used an arbitrary criterion to consider this parameter which is approximately 2 for Modified Gompertz equation. The “lag time” can be determined graphically as the intersection of the tangents to the growth curve at the “lag” and “exponential” phases[16] **(Figure7)**. The Logistic, modified logistic and modified Gompertz showed similar performance. Therefore, the Modified Arrhenius (I) showed the best fitting performance with lowest AIC and RMSE among the models. Noticeably, the $Y_0$, K parameters of the Modified Arrhenius (I) are statistically significant with p-values below 0.05. Hence the Modified Arrhenius (I) model appears to be the best fit model for TVC predication of current study. Comparable to the results of the TVC prediction, the best fit for the Pseudomonas spp population found is Modified Arrhenius (II). While both Modified Arrhenius models have similar RMSE values, Modified Arrhenius II has a significantly lower AIC than Modified Arrhenius I. Furthermore, the RMSE values for Modified Arrhenius (II), logistic, and modified logistic models are all 0.18; however, Modified Arrhenius (II) has a lower AIC value than the other models. As a result, the Modified Arrhenius (II) model appears to be the best fit model for predicting Pseudomonas spp population in this study.

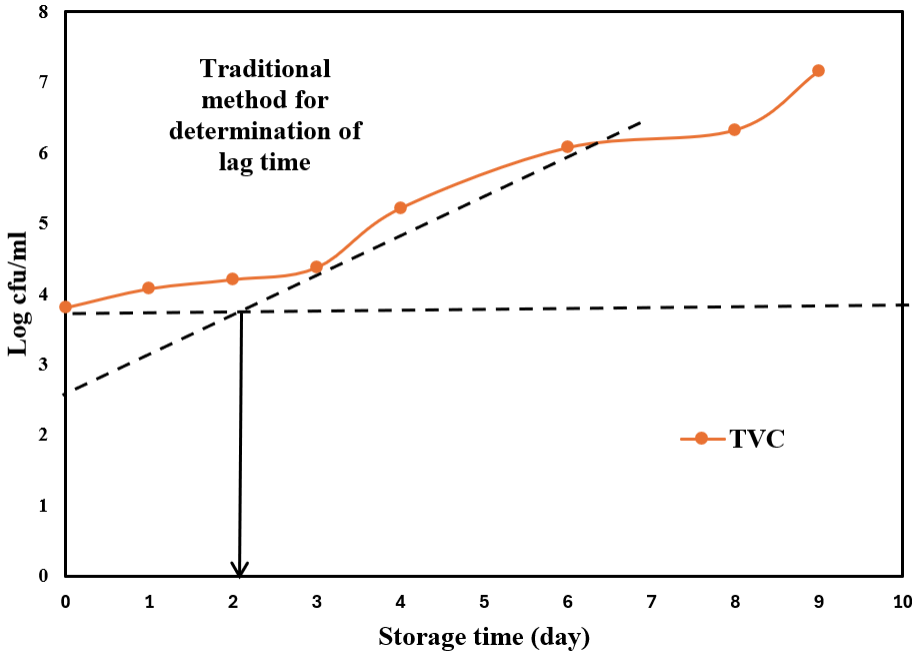


**Figure 7** Traditional method for lag time assumption: $t_0 \sim 2$ day.

**Table 4** Displays the parameter values derived from models based on TVB-N data obtained from the present study.

| **Parameters** | **Exponential** | **Modified Arrhenius (I)** | **Modified Arrhenius (II)** | **Exponential polynomial** | **Modified logistic** | **Howgate** |
|---|---|---|---|---|---|---|
| $Y_0$ | 11.9064 ±3.42 ** | 5.2182 ± 5.49 | 3.28142 ± 4.31 | - | - | - |
| A | - | - | - | 5.6052±2.35 * | 35.3510±2.89 *** | - |
| K | 0.1343±0.04 ** | 3.3437± 0.97** | 6.70694± 2.69 | 0.4912±0.15 ** | 0.8666±0.27 ** | 0.8665±0.27** |
| B | - | - | - | -0.0317±0.01 * | 11.0001±7.86 | - |
| D | - | 1.2406± 2.45 | -0.06392± 0.04 | - | - | - |
| $Y_{max}$ | - | - | - | - | - | 39.8511±2.89 *** |
| $t_d$ | - | - | - | - | - | 2.76±0.36 *** |
| AIC | 43.69 | 41.31 | 39.01 | 37.74 | 34.95 | 34.95 |
| AICc | 55.69 | 81.31 | 79.01 | 77.74 | 74.95 | 74.95 |

| | | | | | | |
|---|---|---|---|---|---|---|
| BIC | 43.06 | 40.48 | 38.18 | 36.90 | 34.11 | 34.11 |
| RMSE | 5.60 | 3.88 | 3.20 | 2.88 | 2.29 | 2.28 |

Level of significance codes: P-value<0.01 ***, P-value<0.05 **, P-value <0.1 *

**Table 5** Displays the parameter values derived from models based on TVC data obtained from the present study.

| **Parameters** | **Modified Arrhenius (I)** | **Modified Arrhenius (II)** | **logistic** | **Modified logistic** | **Modified Gompertz** |
|---|---|---|---|---|---|
| A | - | - | 18.0461±29.29 | 18.0459±29.29 | 53.6758±9.43 |
| K | 0.43±0.07 *** | 0.30±0.10** | 0.1008±0.07 | 0.1008±0.07 | - |
| B | - | | 13.4270±29.21 | 3.8725±7.74 | - |
| D | -1.70±1.89 | 0.02±0.03 | | | |
| $\mu_{Max}$ | | | - | - | 0.6649±0.14*** |

| | | | | | |
|---|---|---|---|---|---|
| $Y_0$ | 3.80±0.22 *** | 3.71±0.20*** | - | - | 0.7894±6.19 |
| AIC | 4.45 | 5.30 | 5.23 | 5.23 | 5.25 |
| AICc | 17.78 | 18.63 | 18.56 | 18.56 | 18.58 |
| BIC | 4.77 | 5.61 | 5.54 | 5.54 | 5.56 |
| RMSE | 0.19 | 0.20 | 0.20 | 0.20 | 0.20 |

Level of significance codes: P-value<0.01 ***, P-value<0.05 **, P-value <0.1 *

**Table 6** Displays the parameter values derived from models based on pseudomonas spp data obtained from the present study.

| **Parameters** | **Modified Arrhenius (I)** | **Modified Arrhenius (II)** | **logistic** | **Modified logistic** | **Modified Gompertz** |
|---|---|---|---|---|---|
| A | - | - | 5.5070±0.27*** | 5.5071±0.27*** | 2.3549±0.5180** |
| K | 0.28090±0.04*** | 0.73090±0.16*** | 0.4385±0.10** | 0.4385±0.10** | - |
| B | 2.19637±1.02 | -0.08645±0.02** | 0.5567±0.31 | 1.2765±0.19*** | - |
| $\mu_{Max}$ | - | - | - | - | 0.7835±0.37 |

| | | | | | |
|---|---|---|---|---|---|
| $Y_0$ | 2.44132±0.32*** | 2.38712 ±0.21*** | - | - | 3.0284±0.3151*** |
| AIC | 7.99 | 3.91 | 4.47 | 4.47 | 15.52 |
| AICc | 27.90 | 23.91 | 24.47 | 24.47 | 35.53 |
| BIC | 7.77 | 3.70 | 4.26 | 4.26 | 15.31 |
| RMSE | 0.24 | 0.18 | 0.18 | 0.18 | 0.55 |

Level of significance codes: P-value<0.01 ***, P-value<0.05 **, P-value <0.1 *

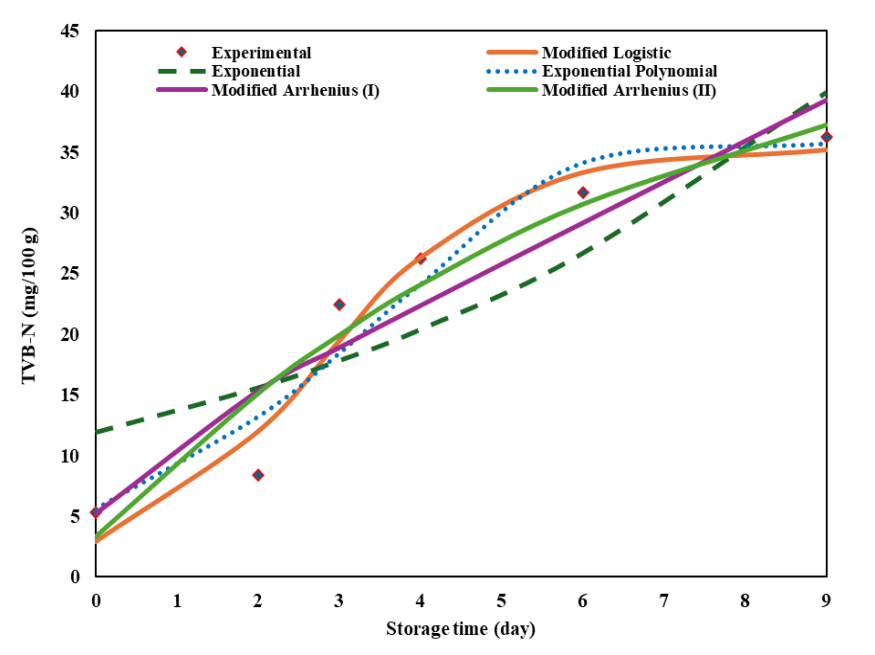


**Figure 8** Different models curve for TVB-N of Pangasius fillets during 4 º C storage for 9 days.

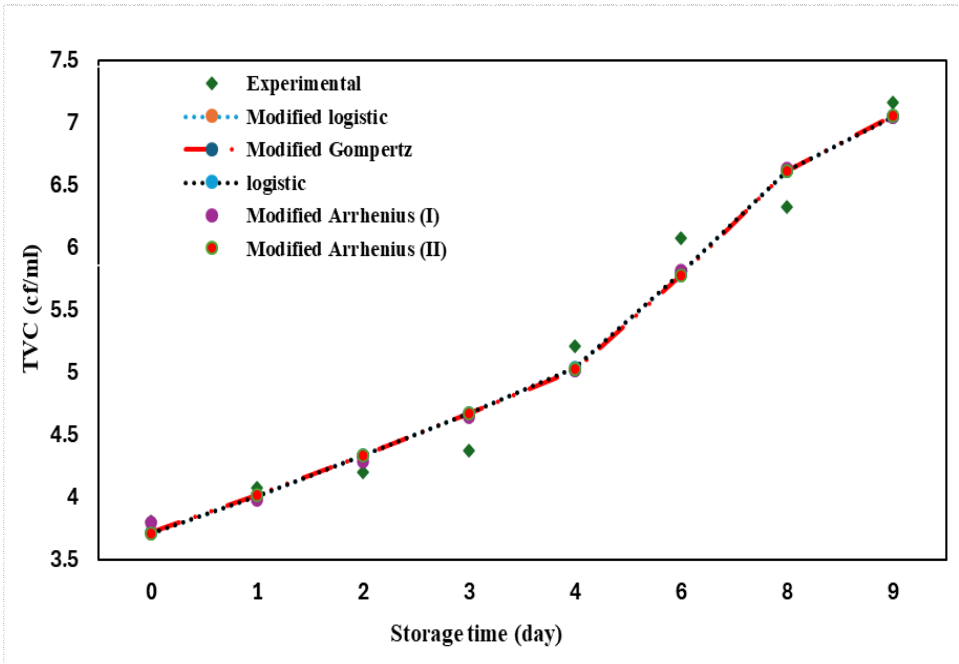


**Figure 9** Different models curve for TVC of Pangasius fillets during 4 º C storage for 9 days.

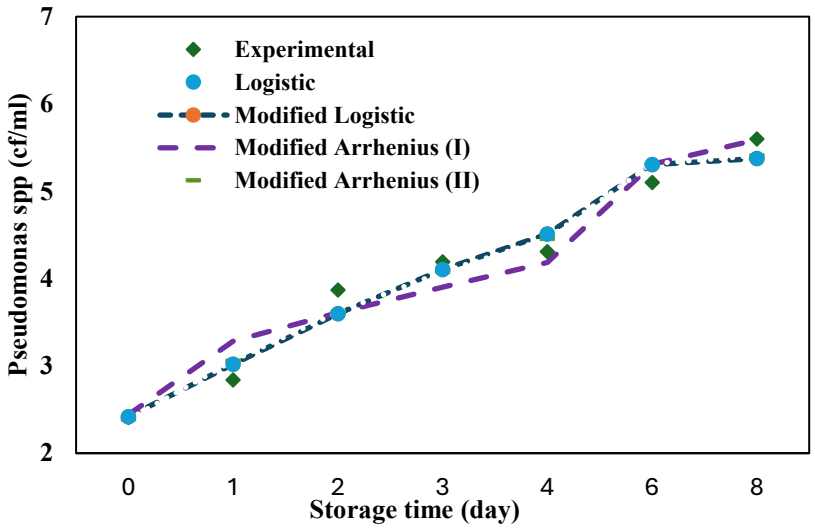


**Figure 10** Different models curve for Pseudomonas spp of Pangasius fillets during 4 º C storage for 9 days.

**Reference**


1. Pimpang P, Sumang R, Choopun S. Effect of concentration of citric acid on size and optical properties of fluorescence graphene quantum dots prepared by tuning carbonization degree. *Chiang Mai J Sci*. 2018;45(5):2005.
2. Sahu M, Reddy VRM, Kim B, et al. Fabrication of Cu2ZnSnS4 Light Absorber Using a Cost-Effective Mechanochemical Method for Photovoltaic Applications. *Materials*. 2022;15(5):1708.
3. Brunchi C-E, Bercea M, Morariu S, Avadanei M. Investigations on the interactions between xanthan gum and poly (vinyl alcohol) in solid state and aqueous solutions. *European Polymer Journal*. 2016;84:161-172.
4. Sun C, Zhang D, Wadsworth LC. Corona treatment of polyolefin films—A review. *Advances in Polymer Technology: Journal of the Polymer Processing Institute*. 1999;18(2):171-180.
5. Yong H, Liu J, Qin Y, Bai R, Zhang X, Liu J. Antioxidant and pH-sensitive films developed by incorporating purple and black rice extracts into chitosan matrix. *International Journal of Biological Macromolecules*. 2019;137:307-316.
6. Mansur A, Rodrigues M, Capanema N, Carvalho S, Gomes D, Mansur H. Functionalized bioadhesion-enhanced carboxymethyl cellulose/polyvinyl alcohol hybrid hydrogels for chronic wound dressing applications. *RSC advances*. 2023;13(19):13156-13168.
7. Ameri M, Ajji A, Kessler S. Characterization of a Food-Safe Colorimetric Indicator Based on Black Rice Anthocyanin/PET Films for Visual Analysis of Fish Spoilage. *Packaging Technology and Science*. 2024;
8. Kassal P, Šurina R, Vrsaljko D, Steinberg IM. Hybrid sol–gel thin films doped with a pH indicator: effect of organic modification on optical pH response and film surface hydrophilicity. *Journal of sol-gel science and technology*. 2014;69:586-595.

9. Ezati P, Rhim J-W, Moradi M, Tajik H, Molaei R. CMC and CNF-based alizarin incorporated reversible pH-responsive color indicator films. *Carbohydrate Polymers*. 2020/10/15/ 2020;246:116614. doi:https://doi.org/10.1016/j.carbpol.2020.116614
10. Hu W, Chen S, Yang J, Li Z, Wang H. Functionalized bacterial cellulose derivatives and nanocomposites. *Carbohydrate Polymers*. 2014/01/30/ 2014;101:1043-1060. doi:https://doi.org/10.1016/j.carbpol.2013.09.102
11. Prabhakar PK, Srivastav PP, Pathak SS, Das K. Mathematical modeling of total volatile basic nitrogen and microbial biomass in stored rohu (Labeo rohita) fish. *Frontiers in Sustainable Food Systems*. 2021;5:669473.
12. Hindle F, Kuuliala L, Mouelhi M, et al. Monitoring of food spoilage by high resolution THz analysis. *Analyst*. 2018;143(22):5536-5544.
13. Ogidi OI, Charles EE, Okore CC, Wilfred B, Oguoma LM, Carbom HE. Mathematical modelling of the growth of specific spoilage microorganisms in tilapia (Oreachromis niloticus) fish. *ASIO J Microbiol Food Sci Biotechnol Innov*. 2021;6(1):09-15.
14. Wang L, Heising J, Fogliano V, Dekker M. Fat content and storage conditions are key factors on the partitioning and activity of carvacrol in antimicrobial packaging. *Food Packaging and Shelf Life*. 2020/06/01/ 2020;24:100500. doi:https://doi.org/10.1016/j.fpsl.2020.100500
15. Yi Z, Xie J. Prediction in the dynamics and spoilage of Shewanella putrefaciens in Bigeye Tuna (Thunnus obesus) by gas sensors stored at different refrigeration temperatures. *Foods*. 2021;10(9):2132.
16. Peleg M, Corradini MG. Microbial Growth Curves: What the Models Tell Us and What They Cannot. *Critical Reviews in Food Science and Nutrition*. 2011/12/01 2011;51(10):917-945. doi:10.1080/10408398.2011.570463